Journal of Cluster Science
https://doi.org/10.1007/s10876-019-01569-w

ORIGINAL PAPER

Facile and Cost-Effective Ag Nanoparticles Fabricated by *Lilium lancifolium* Leaf Extract: Antibacterial and Antibiofilm Potential

Mysoon Al-Ansari[1] · Noorah Alkubaisi[1] · Kasi Gopinath[2] · Viswanathan Karthika[2] · Ayyakannu Arumugam[3] · Marimuthu Govindarajan[4,5]

Received: 8 April 2019

Abstract

In the present study one-pot green fabrication of silver nanoparticles (Ag NPs) with aqueous leaf extract of *Lilium lancifolium*. Synthesized Ag NPs were illustrated by UV–Vis, FT-IR, XRD, AFM and TEM analysis. A surface plasmon resonance peak was noticed at 411 nm in UV–Vis analysis. XRD patterns of Ag NPs showed high crystalline nature with face centered cubic structure. AFM and TEM analysis of Ag NPs exhibit special and anisotropic morphology with accurate particle size about 10–70 nm and average mean value of 45 nm. Ag NPs were tested for antibacterial and anti-biofilm activity against Gram positive and Gram-negative bacterial strains. The exposure to 25 µL exhibited better antibacterial activity and 50 µL significantly control the bacterial biofilm growth. Overall, the proposed green synthesis method of Ag NPs is facile, convenient, less time consuming and environmentally safe.

Keywords *Lilium lancifolium* · Green synthesis · Nanoparticle · AFM and TEM · Antibacterial and antibiofilm activity

Introduction

Since the concept of nanotechnology became famous in the early 1990s, scientists have been developing new techniques by incorporating nanoparticles and nanomaterials into various fields of science. The concept of nanomaterials, although new, has been a part of our civilization since a very long time. Silver nanoparticles (Ag NPs) have been keen attention due to their special properties of size, shape, and self-assembly. They are commonly used in wide range of industries like pharmacology [1, 2], biomedical devices [3, 4], textiles [5, 6], water purification [7, 8] and cosmetics [9, 10]. Many methods are available for synthesis of Ag NPs which include physical, chemical and biological synthesis. In which, biological means of synthesis gained good-attention compared to other two methods due to low cost, simple, environmentally friendly and efficient substitute for the mass production of nanoparticles [11]. In biological methods, Ag NPs are synthesized via using fungus [12, 13], microbes [14, 15] and plants [16–22]. Compare to the fungus and microbes, plants are promising source for nanoparticles production. The advantages of the plant-mediated synthesis of nanoparticles include cost efficient, large-scale production and require low maintenance [23–27]. Important point of using plants in nanoparticles production instead of fungus or bacteria is the lack of pathogenicity [28]. In the past researches, silver nanoparticles are synthesized using extracts from different plant materials such as *Azadirachta indica* [29], *Catharanthus roseus* [30], *Origanum vulgare* [31], *Buddleja*

✉ Mysoon Al-Ansari
soona70@yahoo.com

✉ Marimuthu Govindarajan
drgovind1979@gmail.com

[1] Department of Botany and Microbiology, Female Campus, College of Science, King Saud University, Riyadh, Saudi Arabia

[2] Department of Packaging, Yonsei University, 1 Yonseidae-gil, Wonju-si, Gangwon-Do 26493, South Korea

[3] Department of Botany, Alagappa University, Karaikudi, Tamil Nadu 630 003, India

[4] Unit of Vector Control, Phytochemistry and Nanotechnology, Department of Zoology, Annamalai University, Annamalainagar, Tamil Nadu 608 002, India

[5] Department of Zoology, Government College for Women, Kumbakonam, Tamil Nadu 612 001, India

Published online: 30 April 2019

globosa [32], *Solanum trilobatum* [33] *Gloriosa superba* [34] and etc.

The biofilm is communities of microorganism as well as individual cells are surrounded with exopolysaccharide matrix. This matrix made up of proteins, exopolysaccharides, lipids, RNA and DNA. It has four steps of growing process such as; (1) initial attachment, (2) growth, (3) maturity and (4) dispersion [34, 35]. Biofilms has been a strong resistance, when compared to planktonic cells. Bacterial biofilms are a big issue in the environmental, industrial, and medical field. The organic antibiotic treatment was promoted more resistant behavior of biofilm and to overcome this particular limitation and enhance the antibiofilm activity. Nowadays, material researchers are used to inorganic nanoparticles and nanocomposite materials for polymers, water purification systems, hospital surgical disposables products, because the nanomaterials have the ability to kill pathogenic bacteria [35]. Currently, several attempts had been carried out to in the metal (Ag, Au and Pd) and metal oxide (ZnO, CeO_2) NPs were prevented the bacterial adhesion, and reduced the microbial population [34, 36–38]. Aforementioned metal and metal oxide NPs, the Ag NPs has been showed excellent response to inhibit the bacterial growth, which is due to the size, shape and surface.

Previously various several studies had reported that the Liliaceae family plant have been more sulfur contained bioactive components and amino acids. Based on this ethno-pharmacological understanding, herein we choose the *Lilium lancifolium* for AgNPs synthesis. *L. lancifolium* is a perennial ornamental and edible starch. It is native to Asia, Korea, Japan and China. It is also used for treating pneumonia, bronchitis, chromic gastritis and other pulmonary disorders [39, 40]. It is a fruitful source of chemical diversity, mainly protein, glucomannan, starch, saponin, colchicines [41], flavonoids [42] polysaccharides [43] and phenylpropenoid glycerides [44]. Furthermore, it has been reported for various bioactivities such as antioxidative, antibacterial and anti-inflammatory activities [44–46].

Here, cost-effective Ag NPs were fabricated by *L. lancifolium* leaf extract. The formed Ag NPs were characterized by optical, structural and surface-morphological properties. Furthermore, Ag NPs were investigated into anti-bacterial and anti-biofilm activities.

Materials and Methods

Materials

Lilium lancifolium Thunb. (Fig. 1) leaves were gathered from 405-13, Maeji-ri, Heungeop-myeon, Wonju, Gangwon-do, Republic of Korea. Silver nitrate ($AgNO_3$) obtained from Merck (India), acridine orange, crystal violet, Luria–Bertani broth, Nutrient broth, Nutrient agar media were obtained from HiMedia Laboratories, Pvt. Ltd, India.

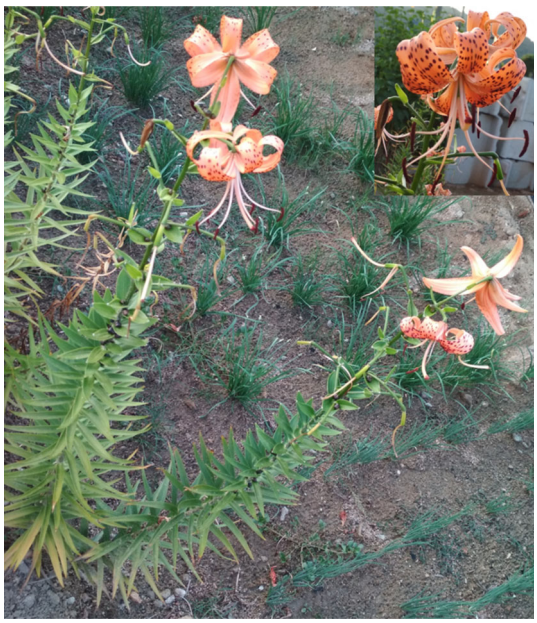

Fig. 1 *Lilium lancifolium*

Synthesis of Ag NPs

Fresh leaves of *L. lancifolium* were sliced into 0.5–1 cm and avoid the mid veins. Then 10 g of sliced leaves were inoculated into 100 ml of boiled water and keep into 10 min. Thereafter, the prepared solution was filtered through Whatman Grade No. 1 filter paper. Then, filtrate was collected in conical flask and stored at room temperature (25 ± 2 °C). Thereafter, 5 ml of *L. lancifolium* leaf extract was introduced in 100 ml of 1 mM Ag NO_3 solution and stirred room temperature at 25 °C. After 3 h, the formation of Ag NPs was confirmed by the colour change of solution from colorless to brown.

Characterization of Ag NPs

UV–visible spectrum of synthesized Ag NPs was analyzed by using Shimadzu UV–visible spectrophotometer (UV-1800, Japan) with the ranging from 300 to 800 nm was used. FT-IR measurements were carried out in the ranging from 400 to 4000 cm^{-1} for transmittance with 16 scan speed with attenuated total reflection mode using diamond/ZnSe (1 reflection) crystal. The structural analysis of Ag NPs was carried out by a powder X-ray diffractometer (PANalytical X' Pert Pro) with Cu-Kα radiation

(wavelength: 1.5418 Å). Surface topology of Ag NPs was analysis using atomic force microscopy (APE Research model no: A100-SGS). The clear morphology with accurate particle size of the sample was examined by high resolution transmission electron microscopy (Tecnai F20 model operated at an accelerating voltage of 200 kV.

Antibacterial Activity

An antibacterial activity of synthesized Ag NPs was analyzed by well diffusion method. The antimicrobial study was carried out using pathogenic bacteria such as *Bacillus subtilis* ATCC 6633 and *Streptococcus pneumoniae*—MTCC 1936 (gram-positive) and *Escherichia coli* MTCC 40 and *Pseudomonas aeruginosa*—MTCC 2642 (gram-negative). The bacteria were cultured in 37 °C nutrient broth until their population reached 1.5×10^8 CFU/mL. Then 20 mL of nutrient agar was poured into the petri dishes and placed it for cool. Bacterial suspension was added in the solidified medium by swabbing method. After swabbing, different concentration of 25, 50 and 100 µL of Ag NPs were introduced by agar plate wells with the help of micropipette. Whereas, 100 µL of *L. lancifolium* leaf extract were used as a negative and 10 µg streptomycin discs as a positive control. All agar plates were incubated at 37 °C for 24 h and an antibacterial was evaluated by measuring the diameter of the inhibition zone around the well. Each experiment was conducted at three times.

Anti-biofilm Activity

Anti-biofilm activity of Ag NPs was assessed by Gram-positive (*Streptococcus pneumoniae*—MTCC 1936) and Gram-negative (*Pseudomonas aeruginosa*—MTCC 2642) bacterial strains. Each bacterial stain was cultured at 37 °C in Luria–Bertani (LB) broth. The sterile glass slides of 1 cm^2 were transferred into 24-well polystyrene plate and each well containing 2.3 mL of LB broth, 50 µl of Ag NPs and 50 µl of bacterial suspension culture 1.6×10^8 CFU/ml. The plate was incubated at 37 °C for 48 h. After 48 h incubation, glass slides were removed and crystal violet (CV) (200 µL of 0.2% CV staining solution (w/v)) staining was performed for the grown biofilm for 10 min and allowed to dry before solubilization of the staining reagent with 1 mL of ethanol. After staining, stained-glass pieces were examined through 40 × magnification with Micro Fire camera (Olympus CX-21i Trinocular Microscope, LED illumination).

Confocal Laser Scanning Microscopy (CLSM) Analysis

To determination of antibiofilm activity, firstly, *S. pneumoniae* and *P. aeruginosa* glass slide was confirmed by the biofilm formation with the help of light microscopic analysis. After 24 h incubation, the Ag NPs treated the biofilm glass were removed from 24-well polystyrene plates and each glass slide was rinsed with three times of 1× phosphate buffered saline (PBS) solution. Then, glass pieces were stained with (0.4%) acridine orange fluorescent dye. Subsequently, they are allowed to dry at room temperature for 3–5 min. Finally, glass slides were subjected to the confocal laser scanning microscopy (CLSM 710, Carl Zeiss, Germany) analysis using an excitation filter of 515–560 nm and each micrograph was taken at 20 × magnification.

Statistical Analysis

The antibacterial activity was described as mean ± standard error (SE) and analyzed using SPSS software. Data normal distribution was confirmed and analysis of variance (One-way Annova) was tested by Turkey's HSD test ($p \leq 0.05$).

Results and Discussion

UV–Vis Analysis of Ag NPs

The *Lilium lancifolium* leaf extract introduce in the Ag NO_3 solution initially the crystal-clear solution was gradually changed into brown color for after 3 h incubation. Based on the visual observation was confirmed by the reduction of Ag^+ into Ag^0. Further the optical, structural and morphological analysis was following below. UV–Vis analysis of leaf extract, Ag NO_3 and synthesized Ag NPs spectra were shown in Fig. 2. The leaf extract and Ag NO_3 solution does not showed any absorbance peak at 400–800 nm region. By introducing the leaf extract into Ag NO_3 solution, we obtained the well absorbance at 411 nm, which is related to the surface plasmon resonance (SPR) of Ag NPs. Generally, the SPR peak shifting also determines the particle. As a blue shift indicates the decreasing the particle size and red shift indicate increase the particle size. During our experiment, we observed that the activation energy was required for synthesis of Ag NPs completed at 3 h. This result was consistent with previous report [47]. However, the time-consuming process for reduction was depending on the plant bioactive components, pH and temperature [48].

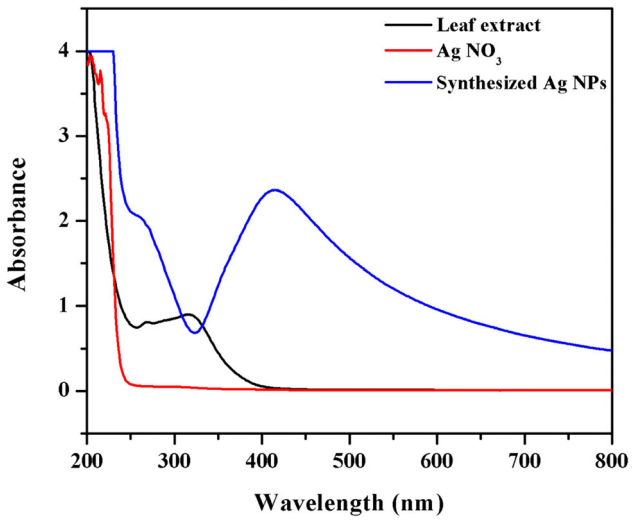

Fig. 2 UV–Vis analysis of *Lilium lancifolium* leaf extract, pure Ag NO_3 and synthesized Ag NPs

FT-IR Analysis of Synthesized Ag NPs

Generally, Fourier transform infrared spectroscopy (FT-IR) analysis have been used for identify the organic and inorganic functional groups. In this study, FT-IR spectrum of leaf extract and synthesized Ag NPs showed multiple strong IR bands, as shown in Fig. 3. The strong bands were observed at 3303, 2131, 1639 and 632 cm^{-1}. The band at 3303 cm^{-1} corresponds to N–H stretching vibration of primary amines. The milled band at 2131 cm^{-1} corresponds to C–N stretching of R–N=C=S. The sharp absorbance band at 1639 cm^{-1}, which could be assigned to N–H stretching and the broad band observed at 632 cm^{-1} is due to the bending vibrations of N–H groups in proteins. Plant extract showed a band observed at 466 correspond to the C–Cl stretching. Evidently, arising these FTIR absorbance band related to the plant bio-active compounds of protein, glucomannan, starch, saponin, colchicines, flavonoids, polysaccharides, phenylpropenoid and glycerides [41–44]. Notably, band disappeared at 466 cm^{-1}, whereas one new band was recorded at 514 cm^{-1} in the synthesized Ag NPs spectrum, which is corresponded to N–H groups in proteins and formation metal (Ag) peak. This observation indicated relatively interaction between the protein and Ag NPs. On the other hand, synthesized Ag NPs spectrum showed a poor transmittance rate compared to leaf extract spectrum, and it also confirmed by the formation of Ag NPs. This decrease transmittance rate was related to a color change of synthesized Ag NPs solution.

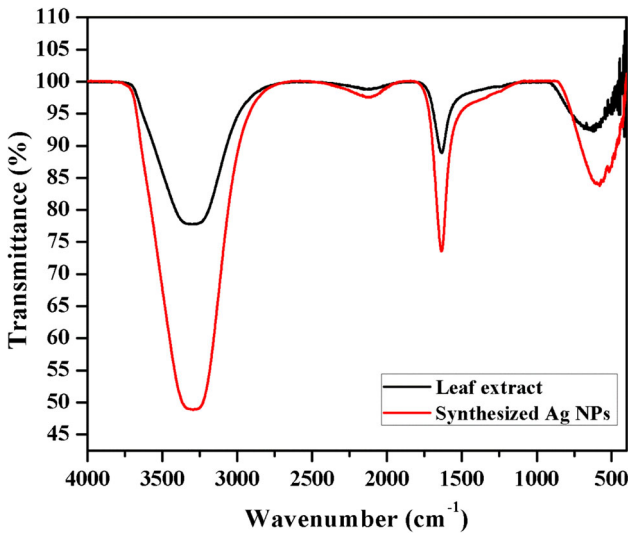

Fig. 3 FTIR spectrum of silver nanoparticles synthesized using aqueous leaf extract of *Lilium lancifolium*

X-ray Diffraction Analysis of Synthesized Ag NPs

The crystal structure of the synthesized Ag NPs was studied by XRD analysis. The XRD result exhibited four distinct diffraction peaks at $2\theta = 38.13°$, 44.31°, 64.44° and 77.37° which were indexed to the planes (111), (200), (220) and (311), respectively, as shown in Fig. 4. This XRD lattice plane of Ag NPs obviously showed high crystalline nature with face-centered cubic structure. The characteristic peak values are well matched with standard data (JCPDS Card No. 89-3722). Nevertheless, the resolved XRD pattern clearly exhibited that the Ag NPs formed by the reduction of Ag^+ ions using *L. lancifolium* leaf extract are crystalline in nature.

AFM and TEM Analysis of Synthesized Ag NPs

Surface topology of the synthesized Ag NPs was studied by AFM analysis. 2D image of Ag NPs showed an apparently

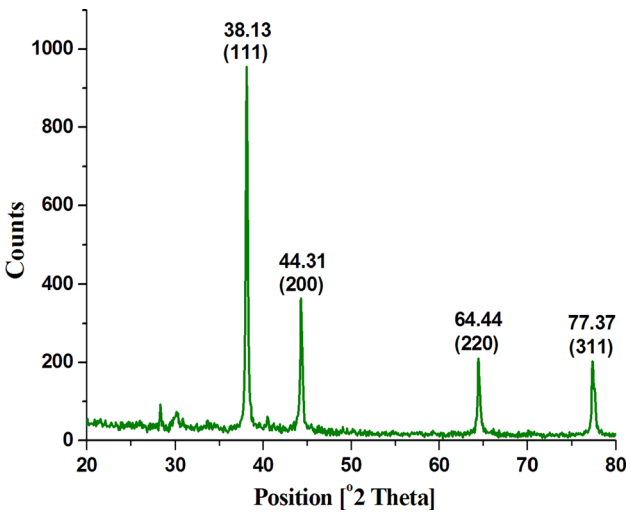

Fig. 4 XRD analysis of synthesized Ag NPs

two different morphology (1) special shape, and (2) anisotropic shape, as shown in Fig. 5a, b. Majority of Ag NPs became a special shape with average diameter of 45 nm, and it also confirmed by the 3D image. The histogram analysis of Ag NPs showed different size particle distribution in the range from 5 to 75 nm, as shown in Fig. 5c. Furthermore, the self-assemble properties of special Ag NPs were showed smooth surface. However, the anisotropic Ag NPs disturb the smooth surface and it is becoming a rough surface, as can be seen in Fig. 5a, b, d. In addition, the exact morphological size and shape of synthesized Ag NPs was confirmed with the help of TEM analysis. Synthesized Ag NPs reveles special and anisotropic shape with the ranging from 5 to 70 nm and it had been an average size of 45 nm, as shown in Fig. 6. Conclusively, synthesized Ag NPs showed heterogeneous dispersion with polycrystalline nature.

Antibacterial Activity

In order to evaluate the antibacterial activity of synthesized Ag NPs was examined against Gram-positive and Gram-negative bacterial strains by well diffusion method. Different concentration of synthesized Ag NPs showed antibacterial activity. As shown in Fig. 7, *B. subtilis, S. pneumoniae* and *P. aeruginosa* were showed excellent antibacterial activity at 25 µL of Ag NPs concentration, when compared to *E. coli* bacteria. Based on the antibacterial activity, over 25 µL Ag NPs does not show any big changes except to *E. coli,* as shown in Fig. 8. Because, antibacterial activity was affected from two reasons such as (1) dose limitation, and (2) diffusion ability. Firstly, does limitation was depended on the minimum inhibitory concentration effect; whereas it was varied form each bacterial species. Secondly, the overloading of Ag NPs in the agar well and migration was blocked by the pore (cavity) of

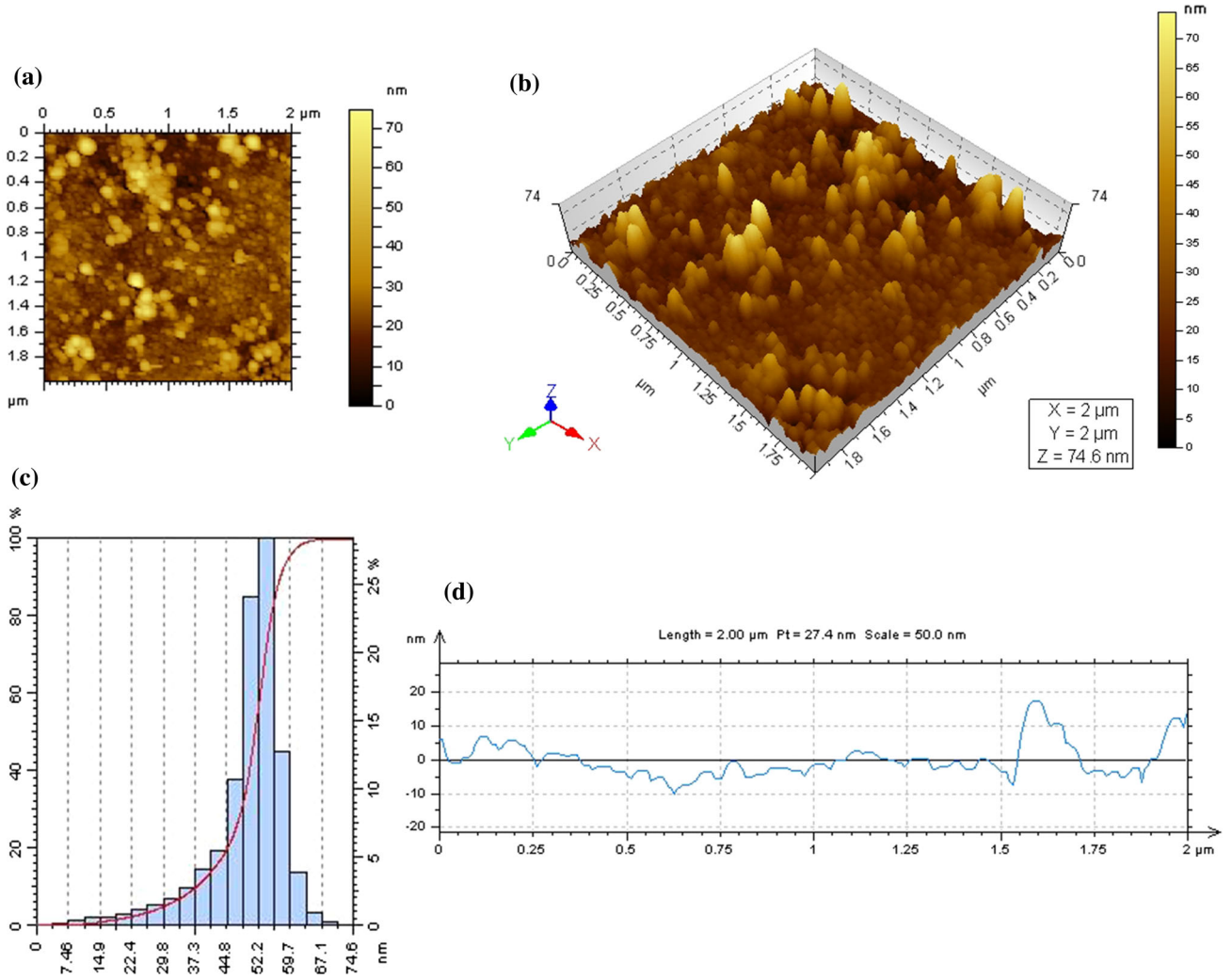

Fig. 5 AFM micrograph; **a**–**b** 2D and 3D image of synthesized Ag NPs, **c** histogram of particle size distribution, **d** line graph of size distribution in synthesized Ag NPs

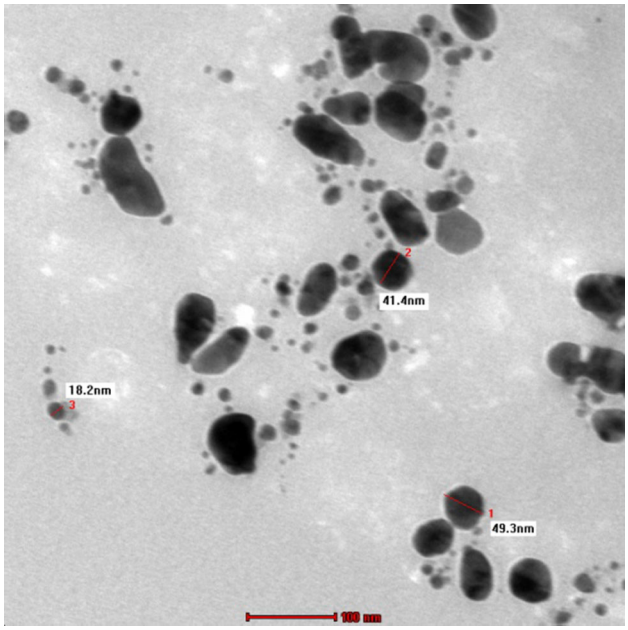

Fig. 6 TEM image of synthesized Ag NPs

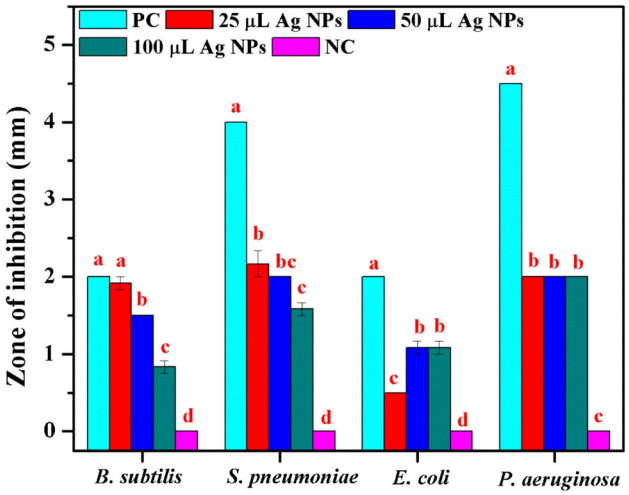

Fig. 8 Antibacterial activity of Ag NPs with different concentration, leaf extract of *L. lancifolium* (NC: negative control) and streptomycin (PC: positive control) against *B. subtilis, S. pneumoniae, E. coli* and *P. aeruginosa*. T-bars represent standard errors. Different letters above each column indicate significant differences (ANOVA, Tukey's HSD test, $P \leq 0.05$)

Fig. 7 Atibacterial activity of Ag NPs

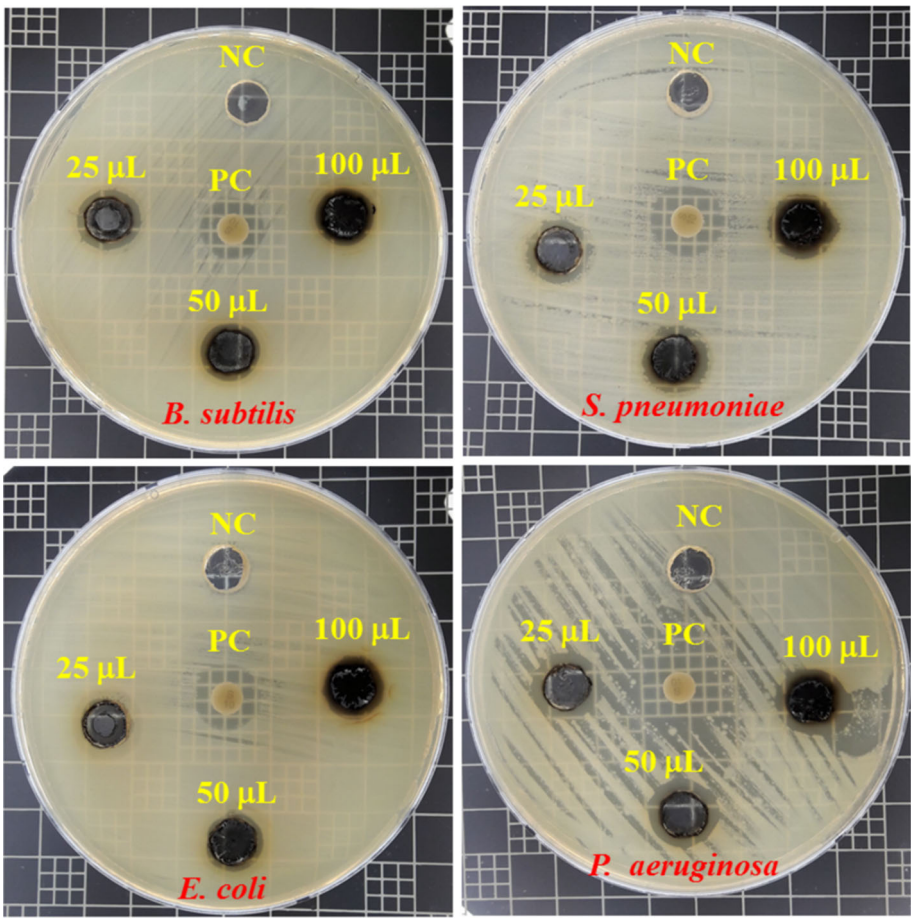

intermolecular residues in polysaccharide (agar), therefore, decreased the diffusion ability with increase the concentration of Ag NPs.

The perfect mechanism of antibacterial activity in metal nanoparticles was tilled now unclarified. Previously, researchers are carried out several attempts in nanoparticles against antibacterial activity. However, some of the scientific reasons are given below; the positively charged nanoparticles interacted with negatively charged bacterial membrane due to the electrostatic bond formation. After this interaction, the Ag NPs are transmitted to the bacterial cytosol. Further, they have easy bind with internal cell organelles mesosomes, endoplasmic reticulum and ribosome sub units and also amino acids, enzymes, metabolic co-factors and anions [34, 47, 49]. Hence, these binding were collapsed the cell intercellular signaling and diminished the metabolic activity of bacterial growth.

Anti-biofilm Activity

To evaluate the antibiofilm activity, the biofilm producing bacterial strains tested for CV and AO staining methods and it was analysis examined by the light and confocal micrographic images. After 48 h treatment, in the control and Ag NPs treated sample of *S. pneumoniae* and *P. aeruginosa* bacterial strain tested with CV staining and it is showed dense and strongly adhesive biofilm formation on the glass substrates, as shown in Fig. 9a, c. Whereas, Ag NPs treated sample showed result was clearly revealed reduction of biofilm bacterial populations as shown in Fig. 9b, d. Further investigation of with and without Ag NPs treated biofilm sample was analyzed with the help of fluorescent dye AO staining. As expected, control sample of *S. pneumoniae* and *P. aeruginosa* AO staining showed dense and strongly adhesive biofilm formation on the glass substrates with thickness of 32 and 26 μm, respectively, as shown in Fig. 10a, c. Ag NPs treated sample was decreased the dens of bacterial growth with thickness of 11 and 7 μm, respectively, as can see in Fig. 10b, d. The same trend was observed at CV staining method, as evident in light micrography images. However, this antibiofilm activity can be explained that (1) Ag NPs can strongly bind to the exopolysaccharides layer due to the electrostatic interaction, (2) Ag NPs can also disrupt the exopolysaccharides structure and adhesiveness, (3) inter and extracellular communication was disrupted by Ag NPs and (4) Ag NPs induced release of radical anions damage the cell membranes. However, Ag NPs interact with sulfur containing amino acids (Methionine and cysteine) resulting in reduction of ATP, lipids, protein synthesis and DNA replication [34, 49, 50]. On account of this consequence, ultimately leading to bacterial cell death and many studies discuss an inhibition of in vitro biofilm formation by different bacterial species at specific nanoparticle concentrations [50]. Previously, Gopinath et al. reported that *Gloriosa superba* mediated synthesis of Ag/Au bimetallic and Ag NPs showed better antibacterial activity against *Bacillus subtilis* and *E. coli* bacterial strains at loading concentration of

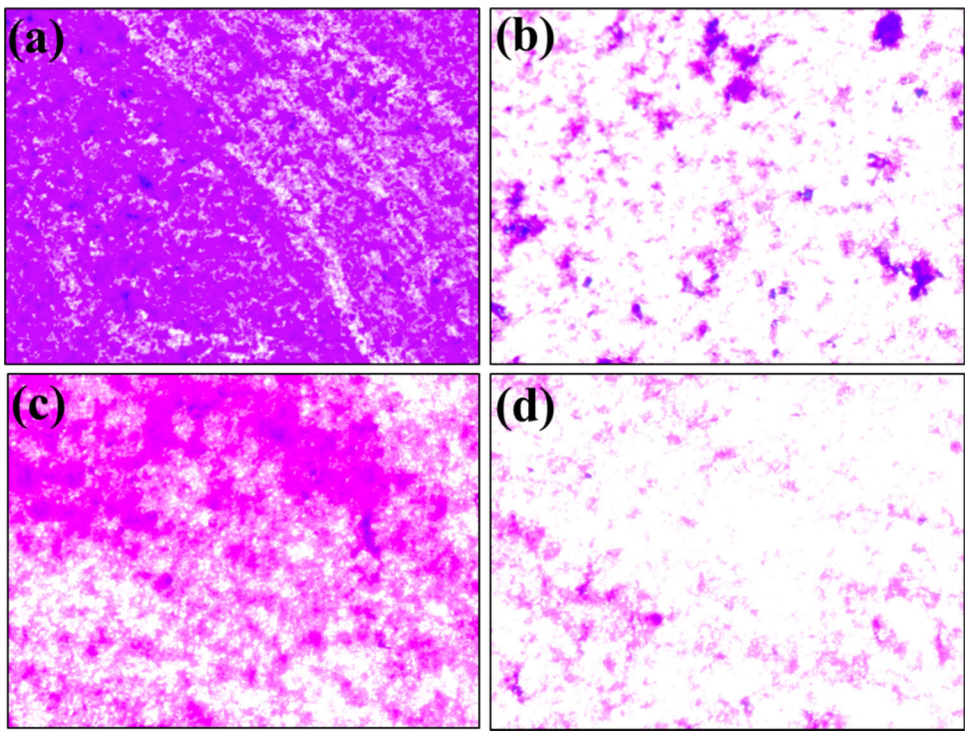

Fig. 9 Antibiofilm activity; crystal violet staining of light microscopy images **a**, **b** control and Ag NPs treatment of *S. pneumoniae,* **c**, **d** control and Ag NPs treatment of *P. aeruginosa*

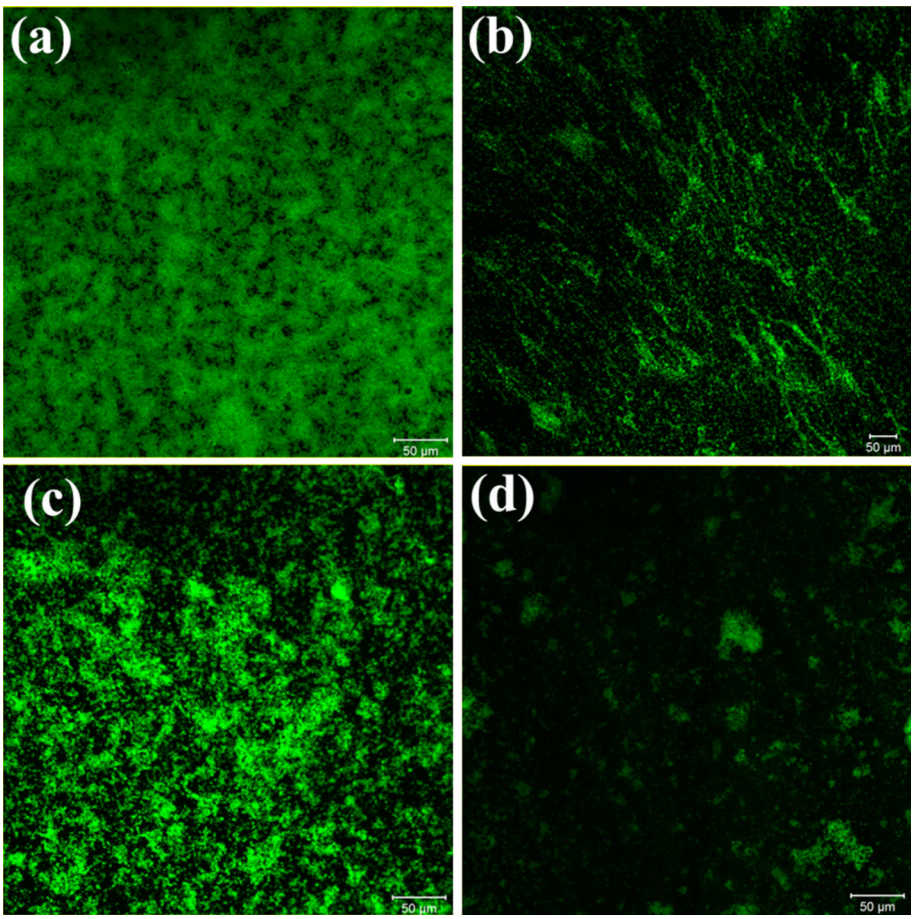

Fig. 10 Antibiofilm activity; acridine orange staining of CLSM images **a**, **b** control and Ag NPs treatment of *S. pneumoniae,* **c**, **d** control and Ag NPs treatment of *P. aeruginosa*

50 µL. At the same time, antibiofilm activity was tested against *Staphylococcus aureus, S. pneumoniae, Klebsiella pneumoniae* and *E. coli* species revealed decreased the biofilm thickness at significant and modulated effect observed in Ag/Au bimetallic and Ag NPs at 250 µL concentration, respectively [34]. In our study, size and shape factor significantly contribute to the excellent antibacterial and antibiofilm activity of the Ag NPs at low concentration of 25 and 50 µL, respectively.

Conclusion

This work was focused on the synthesis of Ag NPs using leaf extract of *Lilium lancifolium*. The synthesized Ag NPs were characterized by optical, structural and morphology properties. UV–Vis and FTIR spectrum of Ag NPs reveled better absorbance at 411 nm and poor transmittance. XRD results exhibit high crystalline nature with face-centered cubic structure. AFM and TEM images demonstrated that the synthesized Ag NPs had special and anisotropic shape with an average size of 45 nm. *B. subtilis, S. pneumoniae* and *P. aeruginosa* was showed excellent antibacterial activity at 25 µL of Ag NPs concentration, except to *E. coli* bacteria. Antibiofilm activity of *S. pneumoniae* and *P. aeruginosa* was showed the inhibition biofilm thickness at 50 µL of Ag NPs concentration, which is clearly evidenced by CV and AO staining images. Henceforth, synthesized Ag NPs can be applied to various fields such as hospital surgical accessories, pharmaceutical products, polymer nanocomposite, adhesive technology, water purification and active food packaging application.

Acknowledgements This research Project was funded by a grant from the Research Center of the Center for Female Scientific and Medical Colleges at King Saud University.

Compliance with Ethical Standards

Conflict of interest The authors declare that they have no conflict of interest.

References

1. N. N. Khatoon, J. A. Mazumder, and M. Sardar (2017). *J. Nanosci. Curr. Res.* **2**, 1–8.
2. P. Mathur, S. Jha, S. Ramteke, and N. K. Jain (2017). *Artif. Cells Nanomed. Biotechnol.* **12**, 1–12.

3. V. Marassi, L. D. Cristo, S. G. J. Smith, S. Ortelli, M. Blosi, A. L. Costa, P. Reschiglian, Y. Volkov, and A. Prina-Mello (2018). *R. Soc. Open Sci.* **5**, 1–21.
4. L. Ge, Q. Li, M. Wang, J. Ouyang, X. Li, and M. M. Q. Xing (2014). *Int. J. Nanomed.* **9**, 2399–2407.
5. D. Ballottin, S. Fulaz, F. Cabrini, J. Tsukamoto, N. Durán, O. L. Alves, and L. Tasica (2017). *Mater. Sci. Eng. C* **75**, 582–589.
6. B. Mahltig, M. Reibold, E. Gutmann, T. Textor, J. Gutmannc, H. Haufe, and H. Haase (2011). *Z. Naturforsch.* **66**, 905–916.
7. M. T. Moustafa (2017). *Water Sci.* **31**, 164–176.
8. N. Savage and M. S. Diallo (2005). *J. Nanoparticle Res.* **7**, 331–342.
9. S. Gajbhiye and S. Sakharwade (2016). *J. Cosmet. Dermatol. Sci. Appl.* **6**, 48–53.
10. S. Kokura, O. Handa, T. Takagi, T. Ishikawa, Y. Naito, and T. Yoshikawa (2010). *Nanomedicine* **6**, 570–574.
11. M. J. Firdhouse and P. Lalitha (2015). *J. Nanotechnol.* **2015**: 1–18, Article ID 829526.
12. X. Zhao, L. Zhou, M. S. R. Rajoka, L. Yan, C. Jiang, D. Shao, J. Zhu, J. Shi, Q. Huang, H. Yang, and M. Jin (2018). *Crit. Rev. Biotechnol.* **38**, 817–835.
13. P. Mukherjee, A. Ahmad, D. Mandal, S. Senapati, S. R. Sainkar, M. I. Khan, R. Parishcha, P. V. Ajaykumar, M. Alam, R. Kumar, and M. Sastry (2001). *Nano Lett.* **1**, 515–519.
14. V. Saklani, V. K. Suman, and K. Jain (2012). *J. Biotechnol. Biomater.* **13**, 1–3.
15. V. L. Das, R. Thomas, R. T. Varghese, E. V. Soniya, J. Mathew, and E. K. Radhakrishnan (2014). *Biotechnology* **4**, 121–126.
16. M. Govindarajan, H. F. Khater, C. Panneerselvam, and G. Benelli (2016). *Res. Vet. Sci.* **107**, 95–101.
17. M. Govindarajan, M. Rajeswary, U. Muthukumaran, S. L. Hoti, H. F. Khater, and G. Benelli (2016). *J. Photochem. Photobiol. B* **161**, 482–489.
18. M. Govindarajan, S. L. Hoti, M. Rajeswary, and G. Benelli (2016). *Parasitol. Res.* **115**, 2685–2695.
19. M. Govindarajan and G. Benelli (2016). *RSC Adv. B* **6**, 59021–59029.
20. G. Benelli and M. Govindarajan (2017). *J. Clust. Sci. B* **28**, 287–308.
21. M. Govindarajan, M. Nicoletti, and G. Benelli (2016). *J. Clust. Sci. B* **27**, 745–761.
22. K. Veerakumar, M. Govindarajan, M. Rajeswary, and M. Muthukumaran (2014). *Parasitol. Res.* **113**, 2363–2373.
23. M. Govindarajan, S. L. Hoti, and G. Benelli (2016). *Enzyme Microb. Technol.* **95**, 155–163.
24. K. Veerakumar, M. Govindarajan, and S. L. Hoti (2014). *Parasitol. Res.* **113**, 4567–4577.
25. M. Govindarajan and G. Benelli (2016). *J. Asia Pac. Entomol.* **19**, 377–385.
26. G. Benelli, M. Govindarajan, S. Senthilmurugan, P. Vijayan, K. Shine, N. S. Alharbi, and J. M. Khaled (2018). *Environ. Sci. Pollut. Res.* **25**, 10283–10293.
27. G. Benelli, F.Maggi, R. Pavela, K. Murugan, M. Govindarajan, B. Vaseeharan, R. Petrelli, L. Cappellacci, S. Kumar, A. Hofer, Youssefi, A. A. Alarfaj, J. S. Hwang, and A. Higuchi (2017). *Environ. Sci. Pollut. Res.* **25**, 10184–10206.
28. N. Pantidos and L. E. Horsfall (2014). *J. Nanomed. Nanotechnol.* **5**, 1–10.
29. S. Ahmed, S. M. Ahmad, B. L. Swami, and S. Ikram (2016). *J. Radiat. Res. Appl. Sci.* **9**, 1–7.
30. S. Ponarulselvam, C. Panneerselvam, K. Murugan, N. Aarthi, K. Kalimuthu, and S. Thangamani (2012). *Asian Pac. J. Trop. Biomed. Trop. Biomed.* **2**, 574–580.
31. M. R. Shaik, M. Khan, M. Kuniyil, A. Al-Warthan, H. Z. Alkhathlan, M. R. H. Siddiqui, J. P. Shaik, A. Ahamed, A. Mahmood, M. Khan, and S. F. Adil (2018). *Sustainability* **10**, 913.
32. E. R. Carmona, N. Benito, T. Plaza, and G. Recio-Sánchez (2017). *Green Chem. Lett. Rev.* **10**, 250–256.
33. M. Vanaja, K. Paulkumar, G. Gnanajobitha, S. Rajeshkumar, C. Malarkodi, and G. Annadurai (2014). *Int. J. Met.* 1–8. Article ID 692461. http://dx.doi.org/10.1155/2014/692461.
34. K. Gopinath, S. Kumaraguru, K. Bhakyaraj, S. Mohan, K. S. Venkatesh, M. Esakkirajan, P. Kaleeswarran, N. S. Alharbi, S. Kadaikunnan, M. Govindarajan, and G. Benelli (2016). *Microb. Pathog.* **101**, 1–11.
35. H. Vlamakis, Y. Chai, P. Beauregard, R. Losick, and R. Kolter (2013). *Nat. Rev. Microbiol.* **11**, 157–168.
36. M. Hazarika, D. Borah, P. Bora, A. R. Silva, and P. Das (2017). *PLoS ONE* **12**, e0184936.
37. M. Abinaya, B. Vaseeharan, M. Divya, A. Sharmili, M. Govindarajan, N. S. Alharbi, S. Kadaikunnan, J. M. Khaled, and G. Benelli (2018). *J. Trace Elem. Med. Biol.* **45**, 93–103.
38. K. S. Venkatesh, K. Gopinath, N. S. Palani, A. Arumugam, S. P. Jose, S. A. Bahadur, and R. Ilangovan (2016). *RSC Adv.* **6**, 42720–42729.
39. E. Lee, N. Yun, Y. P. Jang, and J. Kim (2013). *J. Ethnopharmacol.* **149**, 148–156.
40. X. Yu, J. Zhang, S. Shao, H. Yu, F. Xiong, and Z. Wang (2015). *Starch Stärke* **67**, 448–458. https://doi.org/10.1002/star.201400209.
41. T. Zhang, J. Gao, Z. Y. Jin, X. M. Xu, and H. Q. Chen (2014). *Int. J. Biol. Macromol.* **65**, 436–440.
42. L. X. Niu, Z. N. Li, H. J. Li, and Y. L. Zhang (2017). *Zhongyaocai.* **30**, 85–88.
43. X. You, C. Xie, K. Liu, and Z. Gu (2010). *Carbohyd. Polym.* **81**, 35–40.
44. J. G. Luo, L. Li, and L. Y. Kong (2012). *Food Chem.* **131**, 1056–1062.
45. Y. M. Joung, S. J. Park, K. Y. Lee, J. Y. Lee, J. K. Suh, S. Y. Hwang, K. E. Park, and M. H. Kang (2007). *Korean J. Food Sci. Technol.* **39**, 452–457.
46. O. K. Kwon, M. Y. Lee, J. E. Yuk, S. R. Oh, Y. W. Chin, H. K. Lee, and K. S. Ahn (2010). *J. Ethnopharmacol.* **130**, 28–34.
47. V. Karthika, A. Arumugam, K. Gopinath, P. Kaleeswarran, M. Govindarajan, N. S. Alharbi, S. Kadaikunnan, J. M. Khaled, and G. Benelli (2017). *J. Photochem. Photobiol. B* **167**, 189–199.
48. A. A. Kajani, A. K. Bordbar, S. H. Z. Esfahani, A. R. Khosropour, and A. Razmjou (2014). *RSC Adv.* **4**, 61394–61403.
49. K. Gopinath, S. Gowri, and A. Arumugam (2013). *J. Nanostruct. Chem.* **3**, 68.
50. K. Markowska, A. M. Grudniak, and K. I. Wolska (2013). *Acta Biochim. Pol.* **60**, 523–530.